RSC Advances

PAPER

View Article Online
View Journal | View Issue

Cite this: *RSC Adv.*, 2021, **11**, 17648

Role of oxide support in Ni based catalysts for CO_2 methanation

Ye Hwan Lee,[a] Jeong Yoon Ahn,[a] Dinh Duc Nguyen, [b] Soon Woong Chang,[b] Sung Su Kim *[b] and Sang Moon Lee *[b]

Received 24th March 2021
Accepted 7th May 2021

DOI: 10.1039/d1ra02327f

rsc.li/rsc-advances

The CO_2 methanation reaction of reduced and unreduced Ni based CeO_2, Al_2O_3, TiO_2 and Y_2O_3 supported catalysts was investigated. The Ni/CeO_2 and Ni/Y_2O_3 catalysts exhibited similar CO_2 conversions at all reaction temperatures. The catalysts were studied by X-ray diffraction (XRD), H_2 chemisorption, H_2 temperature-programmed reduction (TPR), and *in situ* diffuse reflection infrared Fourier transform spectroscopy (DRIFTS); the results suggested that the reducibility of both metal and support at low temperature, strong metal support interaction and small Ni particle size are important factors for low-temperature CO_2 methanation. Based on the DRIFT studies, the difference in the CO_2 adsorption properties and reaction pathway depending on the reduced and unreduced Ni based supported catalysts was discussed.

1 Introduction

The CO_2 methanation reaction is important in industry because it produces methane and removes CO_2. Among the CO_2 conversion reactions using catalysts, the CO_2 methanation reaction or so-called Sabatier reaction, is the most advantageous reaction.[1] CO_2 methanation is a simple reaction which makes it possible to integrate the transformation of methane into biogas through the process of anaerobic digestion to generate power, or into other industrial plants with CO_2-rich exhaust gases.[2] CO_2 methanation is a highly exothermic reaction, and it can produce the heat. CO_2 methanation also has a large equilibrium constant at a lower temperature, so that methane can be generated with a high conversion at lower temperatures; however, the conversion was still low due to kinetic limitation and catalyst performance. Catalytic performance is dependent on various parameters, such as the kinds of support, preparation methods, and the addition of promoters.[3] Especially, many researchers have studied the effect of support to enhance the performance of the CO_2 methanation reaction. The support has a significant effect on the redox properties, metal–support interaction, metal dispersion and adsorption properties.[4–6] Many efforts have been made to develop Ni-based supported catalysts for low-temperature CO_2 methanation.[7–11] The CO_2 methanation activity has been investigated using Ni-based catalysts deposited on various supports such as SiO_2,[12] α-Al_2O_3,[13] MgO,[14] ZrO_2,[15] Y_2O_3,[16] CeO_2,[17] TiO_2,[18] β-zeolite,[19] and their composite supports such as Ni/CeO_2–ZrO_2,[20] Ni/γ-Al_2O_3–ZrO_2–TiO_2–CeO_2,[21] Ni/CeO_2–Al_2O_3.[22] Frontera *et al.*[23] reported that the catalytic activity strongly effects on the characteristics of the support for Ni based catalysts. Le *et al.*[24] founded that the high Ni dispersion and strong CO_2 adsorption plays an important role in the high CO and CO_2 methanation activities for Ni/CeO_2 catalyst. Tada *et al.*[13] reported that the Ni/CeO_2 catalyst showed a high conversion compare to Ni/α-Al_2O_3. A large CO_2 adsorption amount and high CO_2 reduction ability could result in high CO_2 conversion at a low temperature using a Ni/CeO_2 catalyst. Muroyama *et al.*[16] found that the Ni/Y_2O_3 catalyst exhibited a high CO_2 conversion and CH_4 yield compare to Ni/CeO_2, Ni/Al_2O_3, Ni/ZrO_2, Ni/La_2O_3 and Ni/Sm_2O_3 catalysts. They expected that the promotion of the decomposition of formate species would lead to high catalytic activity. Abello *et al.*[25] have reported that the Ni–Al-activated catalyst prepared by a co-precipitation method exhibited a high CO_2 conversion and stability at a high space velocity and highly loaded and dispersed small Ni nanoparticles (*ca.* 6 nm) dispersed over NiO–alumina by partial reduction of the mixed oxide. Vogt *et al.*[26] reported that CO_2 hydrogenation over Ni is considered to follow two steps; direct dissociation and H-mediated and they proved how structure sensitivity effects the mechanism of CO_2 hydrogenation over Ni/SiO_2. Zeolite and TiO_2 supports are also used as Ni catalysts during CO_2 methanation. Liu *et al.*[18] reported that the 15 wt% Ni/TiO_2 catalyst prepared by deposition–precipitation method showed excellent CO_2 methanation activity (conversion: 96%; selectivity: 99%) at 260 °C. The good dispersion of Ni particles with high exposure of active sites, which may lead to enhanced exposure of active sites that facilitate the generation of surface-dissociated hydrogens. Recent reports have shown substantial improvement in the CO_2

---

[a] *Department of Environmental Energy Engineering, Graduate School of Kyonggi University, 94-6 San, Iui-dong, Youngtong-ku, Suwon-si, Gyeonggi-do, 442-760, Korea*

[b] *Department of Environmental Energy Engineering, Kyonggi University, 94-6 San, Iui-dong, Youngtong-ku, Suwon-si, Gyeonggi-do, 442-760, Korea. E-mail: sskim@kyonggi.ac.kr; leesangm@kyonggi.ac.kr*

methanation rate by changing the support's properties and/or by the addition of promoters such as Ni–W–Mg,[27] Ni–La,[28] Ni–Cu or Fe/Al_2O_3 (ref. 29) catalysts. Many studies have examined the performance of highly active Ni-based catalysts supported on various metal oxides for CO_2 methanation at low temperature. However, the effect of metal–support interaction and role of support on catalytic performances during Ni based CO_2 methanation reaction is yet to be unraveled. In this work, CeO_2, Y_2O_3, TiO_2 and Al_2O_3 supports were selected as representative Ni catalysts and prepared by wet impregnation method. We investigated the catalytic activities of all catalysts for CO_2 methanation and examined their physicochemical properties. Moreover, the adsorbed species on the reduced and unreduced catalyst surface were compared.

2 Experimental

2.1 Preparation of catalysts

Ni-Based catalysts supported on CeO_2 (Sigma Aldrich Co.), α-Al_2O_3 (Alfa Aesar Co.), Y_2O_3 (Sigma Aldrich Co., St. Louis, MO, USA) and TiO_2 (G-5, Cristal Global Co.) were prepared by a wet impregnation method. Nickel nitrate hexahydrate ($Ni(NO_3)_2 \cdot 6H_2O$; Sigma Aldrich Co.) was dissolved in distilled water at 80 °C. After impregnation, the moisture was removed at 80 °C using a rotary vacuum evaporator and then dried at 103 °C oven for 12 h. The samples were calcined at 400 °C for 2 h and then samples were reduced at 420 °C for 2 h with a 30% H_2/N_2. The obtained samples were grounded and sieved using a 40–50 mesh. Ni loading was fixed at 10 wt%.

2.2 Catalytic activity

The CO_2 methanation experimental apparatus consisted of a continuous flow-type fixed-bed reactor comprising a quartz tube (inner diameter: 8 mm; height: 600 mm) and a catalytic bed (Fig. 1). To measure the gas temperature, another K-type thermocouple was installed at the top of the catalytic bed. Prior to the experiment, the catalysts were pretreated at 420 °C for 1 h with a 30% H_2/N_2 at a flow rate of 100 $cm^3\ min^{-1}$. The feed gases comprised 16.67% CO_2, 66.66% H_2 and 16.67% N_2. The total flow through the reactor was 120 $cm^3\ min^{-1}$ and a space velocity of 14 400 $l\ kg^{-1}\ h^{-1}$ was obtained. The outlet gas-supply pipe was made of stainless steel and wrapped with a heating band set at 180 °C to prevent water condensation. The concentrations of the reactants and products were measured as follows: the inlet and outlet gas concentration were analyzed using a gas chromatograph with a thermal conductivity detector (GOW-MAC, series 580). The CO_2 conversion and yield can be calculated as the following:

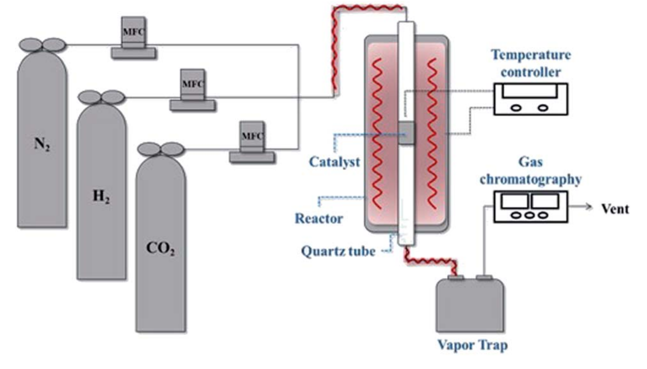

Fig. 1 Schematic of the experimental fixed bed catalytic reactor for CO_2 methanation.

$$CO_2\ \text{conversion}\ (\%) = \frac{(CO_{2\text{in}} - CO_{2\text{out}})}{CO_{2\text{in}}} \times 100$$

$$CH_4\ \text{yield}\ (\%) = \frac{CH_{4\text{out}}}{CO_{2\text{in}}} \times 100$$

$$CO\ \text{yield}\ (\%) = \frac{CO_{\text{out}}}{CO_{2\text{in}}} \times 100$$

2.3 Characterization

The surface areas of Ni based catalysts were obtained by the Brunauer–Emmett–Teller (BET) equation using an ASAP 2010 instrument (Micrometrics). The Ni dispersion was evaluated by H_2 chemisorption at 35 °C using a Micrometrics ASAP 2020 instrument (Micrometrics). All catalysts were reduced under a H_2 airflow at 300 °C for 1 h and then cooled into 35 °C. X-Ray diffraction (XRD) analysis was measured on an X'Pert PRO MRD instrument (PANalytical) with a Cu Kα ($\lambda = 1.5056$ Å) radiation. Field emission-transmission electron microscope (TEM) analysis was carried out on a JEM-2100 F (JEOL) microscope (200 keV voltage). All samples were prepared by suspending an ultrasonicated catalyst powder in ethanol and placing the suspension on a Cu grid. For H_2 chemisorption analysis, the catalysts were activated with 10% H_2 at 300 °C for 0.5 h and then cooled to 50 °C and saturated with H_2 pulses. The temperature-programmed reduction (TPR) of H_2 was measured by 10% H_2/Ar using 0.3 g of the catalyst at a total flow rate of 50 $cm^3\ min^{-1}$. Before the H_2 TPR measurement, the catalyst was pretreated in a flow of air at 400 °C for 0.5 h, followed by cooling to 50 °C. The catalyst was placed in dilute hydrogen, and the consumption of hydrogen was monitored using Autochem 2920 (Micrometrics) by increasing the temperature to 900 °C at a rate of 10 °C min^{-1}. X-ray photoelectron spectroscopy (XPS) analysis was performed using an ESCALAB 210 (VG Scientific), and Al Kα monochromate (1486.6 eV) was used as an excitation source. Fourier-transform infrared (FT-IR) spectroscopy experiments were conducted in a diffuse reflection cell equipped with a CaF_2 window using an FT-IR spectrometer (Nicolet IS 10, Thermo-Fisher), and diffuse reflectance (DR) 400 accessory was used. The spectra included 30 accumulated scans at resolutions of 4 cm^{-1}, which were obtained using a mercury–cadmium–telluride (MCT) detector. To investigate the characteristics of CO_2 adsorption and CO_2 methanation reaction, the gas flowing over the samples pretreated by H_2 and air were switched to CO_2 or $CO_2 + H_2$ for 20 min at 200 and 300 °C.

3 Results and discussion

3.1 Catalytic activities

Fig. 2 shows the CO_2 conversions of Ni-based catalysts supported on CeO_2, TiO_2, Y_2O_3 and Al_2O_3 at different reaction temperatures for the CO_2 methanation reaction. Among the catalysts, the reduced Ni/CeO_2 and Ni/Y_2O_3 catalysts exhibited the similar CO_2 conversion over a range from 250 to 400 °C. For the reduced Ni/Al_2O_3 catalyst, the CO_2 conversion decreased at 250–280 °C and then reached the maximal value at 350–380 °C. Especially, the Ni/TiO_2 catalyst exhibited a very poor CO_2 conversion at all temperature range. The CO_2 to CH_4 and CO conversions are also shown in Fig. 2(b) and (c). CO_2 was fully converted to the CO (0.1–2.1%) in all temperature range for Ni/TiO_2 catalyst. From the properties of the equilibrium conversion, the reverse water gas shift reaction is not favored at a low temperature. Thus, it is indicated that the CO_2 should be able to convert CO on the reduction sites on a TiO_2 support. Except for the Ni/TiO_2 catalyst, CO yields were nearly zero at a reaction temperature under 300 °C, indicating that all CO_2 conversion is mostly concordant with CO_2 conversion to CH_4. The order of catalytic activity regardless of the reaction temperature was as follows: Ni/CeO_2 $\approx$ Ni/Y_2O_3 > Ni/Al_2O_3 > Ni/TiO_2. It could be concluded that the reduced Ni/CeO_2 and Ni/Y_2O_3 catalysts showed superior activity at a low temperature. Although catalytic activity of the Ni-based catalyst differs with operation conditions such as temperature, pressure, catalyst loading, and gas component, the general results showed similarities to previously reported studies by other researchers.[11,30,31] Cai *et al.*[30] reported that CO_2 conversion of Ni/$Ce_xZr_{1-x}O_2$ catalyst showed the 72.21% at 390 °C. The higher reducibility of the Ce-rich supported highly-dispersed Ni catalyst was considered to be an important factor for long-term stability.[30,32,33] However, the role of Ni dispersion in the stability of the Ni/CeO_2 catalyst is difficult to elucidate in this work, and further studies will be necessary to fully address this point.

3.2 Physicochemical properties

The BET surface areas and metal dispersions of the reduced and unreduced samples are summarized in Table 1. The order of support's surface area was as follows: TiO_2 > CeO_2 > Al_2O_3 > Y_2O_3 (TiO_2: 316.226, CeO_2: 29.557, Al_2O_3: 7.375, Y_2O_3: 2.615 $m^2\ g^{-1}$; not shown in the figure). It can be observed that the Ni/TiO_2 catalyst had a much larger specific surface area than other catalysts. Zhang *et al.*[34] showed that the catalyst's specific surface area is not directly related to the catalytic activity in CO_2 methanation for Ni-based catalysts. Our results were in good agreement with previously mentioned evidence from the literature. The reduced Ni/TiO_2 catalyst had the lowest value of Ni dispersion (0.0116%). The reduced Ni/Y_2O_3 catalyst showed the highest metal dispersion (2.7883%) of all the unreduced Ni-

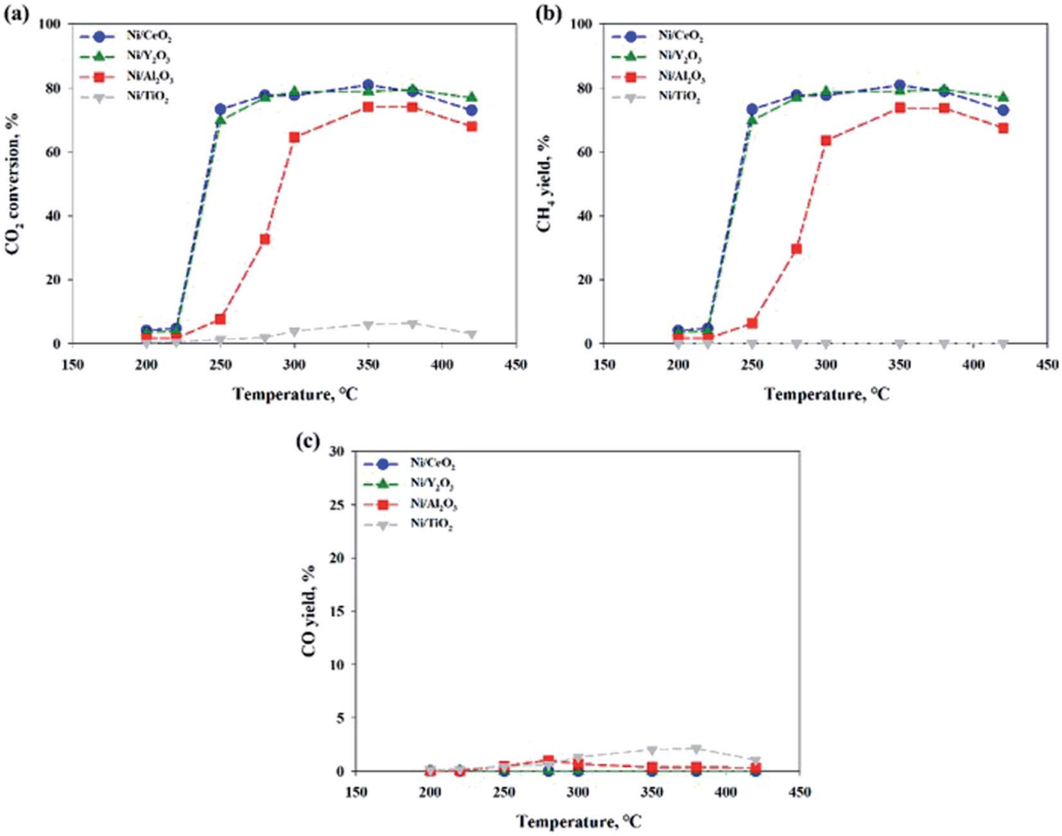

Fig. 2 (a) CO_2 conversions, (b) CH_4 and (c) CO yield in CO_2 methanation over 10 wt% Ni/support catalysts. $CO_2 : H_2 : N_2 = 1 : 4 : 1$, GHSV: 14 400 l $kg^{-1}\ h^{-1}$.

Table 1 BET surface area and metal dispersion of reduced and unreduced Ni/metal oxide catalysts

	Surface area ($m^2\ g^{-1}$)		Metal dispersion[a] (%)	
	Unreduced	Reduced	Unreduced	Reduced
Ni/CeO_2	29.907	22.845	4.932	1.823
Ni/Y_2O_3	16.794	21.233	3.438	2.788
Ni/Al_2O_3	9.867	8.698	2.323	0.027
Ni/TiO_2	121.74	43.606	0.067	0.012

[a] Calculated by H_2 pulse chemisorption.

based catalysts. Reduction degree of surface area and metal dispersion for Ni based catalysts with heat treatment by air or H_2 can be attributed to complex interdependency on metal–support interactions. This would suggest that a decrease of metal dispersion by reduction treatment could be explained by a strong interaction between Ni and oxide support. The order of strength of the metal and support interaction was as follows: $Ni/Al_2O_3 < Ni/TiO_2 < Ni/CeO_2 < Ni/Y_2O_3$. Fig. 3(a)–(d) shows the XRD patterns of raw supports, calcined supports, calcined Ni based catalysts and calcined Ni based catalysts. The XRD pattern of Ni consists of three main peaks at 45°, 53°, and 76° corresponding to (111), (200), and (220) planes, respectively. The XRD pattern of NiO consists of two main peaks at 37° and 62° corresponding to (111) and (220) planes, respectively.[35] For the TiO_2 powder, the main peaks were observed to be at $2\theta = 25.3$, 37.1 and 47.5°, corresponding to typical anatase TiO_2 peaks. The sharp peaks were observed for the crystallite TiO_2 structure when the amorphous TiO_2 powder was calcined at a temperature of 400 °C. NiO peaks were not observed in calcined Ni/TiO_2 catalyst. It is interesting to note that Ni crystallite main peaks were detected at $2\theta =$ at 44.5, 51.8 when using the reduced Ni/TiO_2 catalyst. The release of bonding oxygen atoms within Ni–O–Ti by H_2 reduction will help to move the Ni particles, then the Ni particles are easily agglomerated. Ni and NiO peaks were observed in both reduced and unreduced Ni/Al_2O_3 catalysts. Unlike the Ni/TiO_2 catalyst, it confirmed that Ni and NiO particles were agglomorated by heat treatment regardless of the migration of oxygen atom for Ni supported on irreducible Al_2O_3. CeO_2 and Y_2O_3 support had quite low surface area. Nevertheless, the Ni and NiO peaks were not observed in reduced and unreduced Ni/Y_2O_3 catalyst and very low Ni and NiO peaks were observed in reduced and unreduced Ni/CeO_2 catalyst, which is related to strong metal–support interactions (SMSI effect). This phenomenon is in agreement with results from previous metal dispersion. TEM analysis was conducted to estimate the Ni particle sizes of Ni based catalysts. The TEM and mapping images of the reduced Ni catalysts are presented in Fig. 4(a)–(l). It could be seen that the Ni/Y_2O_3 mean particle size of Ni was 12.8 nm, while that of Ni/CeO_2, Ni/Al_2O_3 and Ni/TiO_2 were 16.5 nm, 19.9 nm and 21 nm, respectively. Vogt *et al.*[25] investigated the particle size effect of Ni/SiO_2 catalysts prepared by

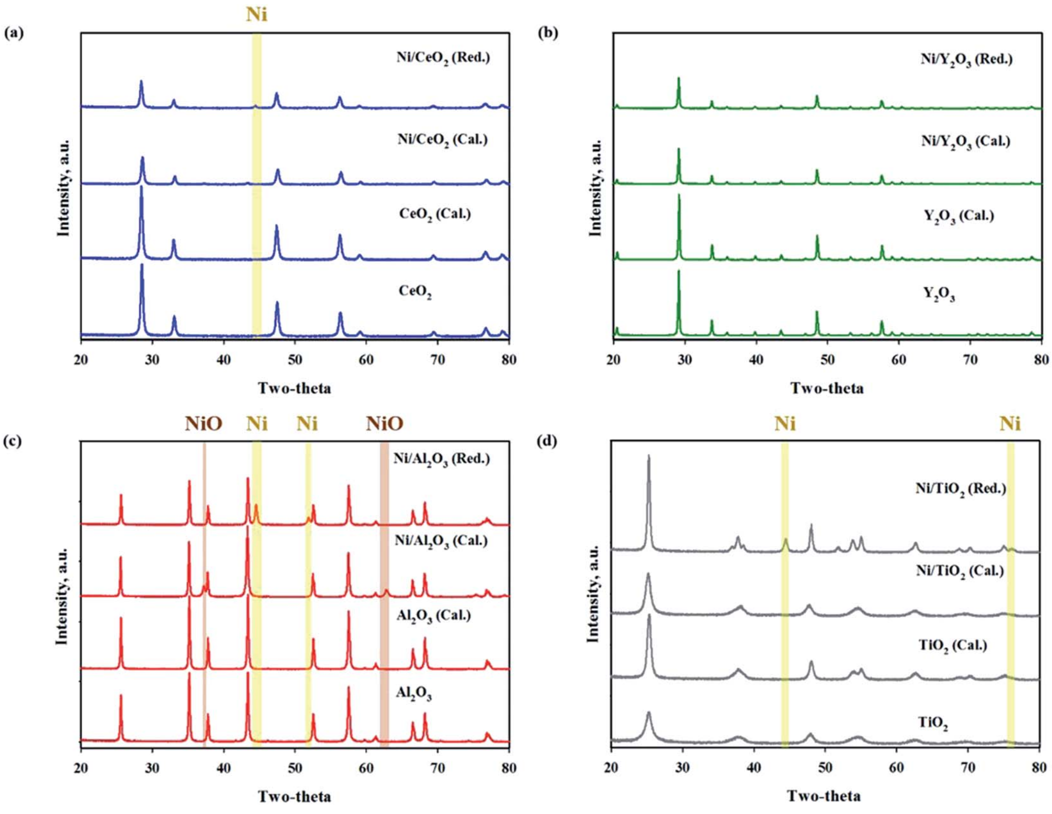

Fig. 3 XRD patterns of metal oxide supports and reduced (red.) and unreduced (cal.) Ni supported catalysts ((a) Ni/CeO_2, (b) Ni/Y_2O_3, (c) Ni/Al_2O_3, (d) Ni/TiO_2).

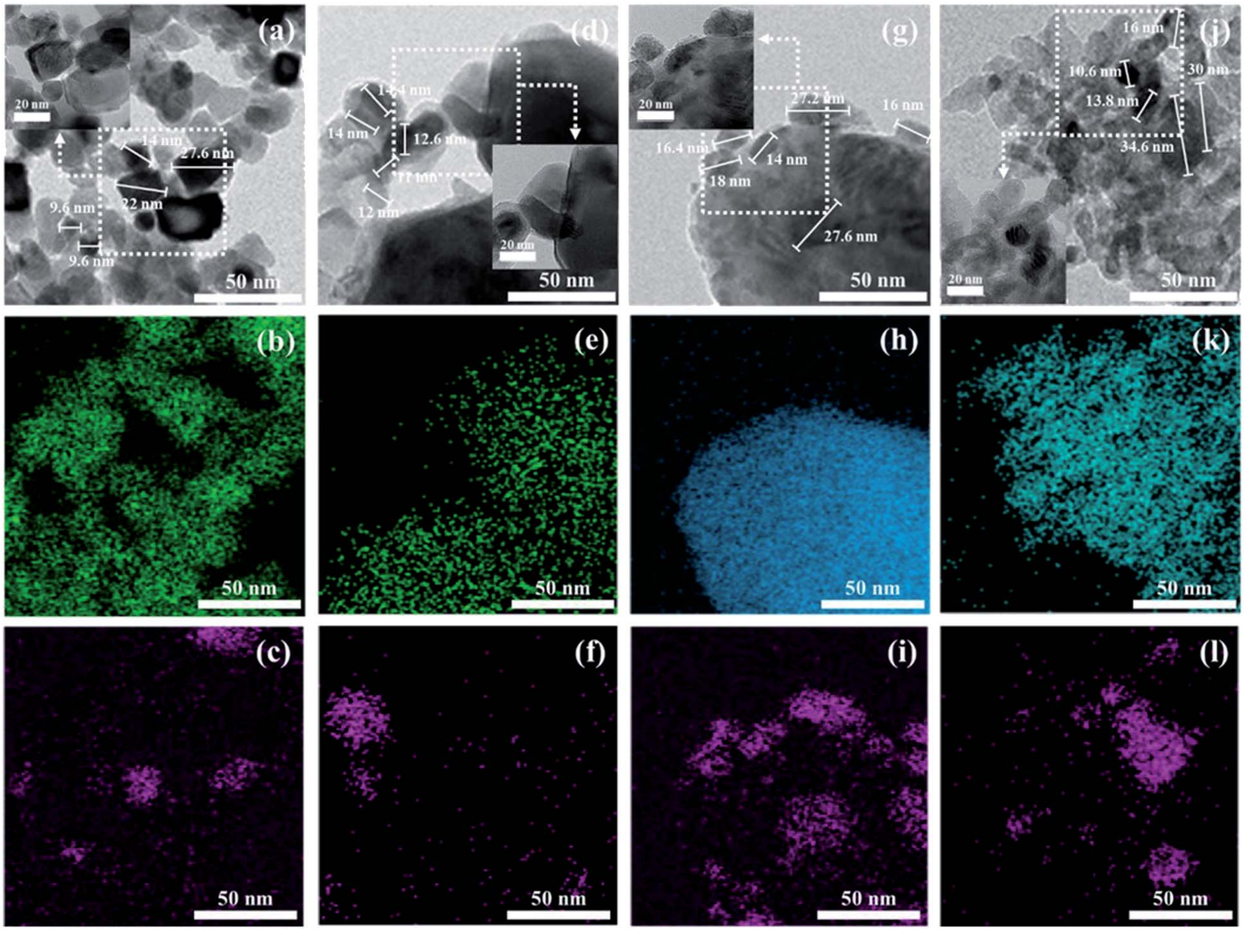

Fig. 4 TEM and mapping images of Ni/support catalysts ((a) Ni/CeO_2, (b) Ce, (c) Ni, (d) Ni/Y_2O_3, (e) Y_2O_3, (f) Ni, (g) Ni/Al_2O_3, (h) Al_2O_3, (i) Ni, (j) Ni/TiO_2, (k) TiO_2, (l) Ni).

homogeneous deposition precipitation and co-precipitation with different Ni loadings (1–60 wt%). It was concluded that the Ni based CO_2 methanation is structure sensitive from 1–7 nm for Ni/SiO_2 catalyst. Many studies have attempted to enhance the Ni dispersion by increasing H_2 adsorption as active sites.[11,36–39] In this study, the 10 wt% Ni-based catalysts prepared by the impregnation method have relatively large Ni particle size of 12.8–21 nm, but it has low temperature CO_2 methanation activity. In the case of Ni/Al_2O_3 and Ni/TiO_2 catalyst, it was confirmed that the difference in activity at high temperature (280–420 °C) was clearly displayed despite the similar particle size and metal dispersion. The fact that the Ni particles play an important role in the adsorption of hydrogen as active sites, but other factors such as CO_2 adsorption characteristics and oxygen transfer by hydrogen can influence the catalytic performance.

The reducibility of Ni-based catalysts was investigated by a H_2-temperature programmed reduction, and the profiles are shown in Fig. 5(a). A similar H_2-TPR result for the Ni/CeO_2 catalyst was previously reported.[13,17,40] Zhou *et al.*[17] reported that three reduction peaks can be seen at around 220 °C, 280–330 °C and 380 °C. The first low temperature peak attributed to the reduction of highly dispersed NiO species. The second peak attributed to the reduction of NiO species on the subsurface of the Ni/CeO_2 catalyst and highly dispersive NiO species. The last peak can be assigned to the reduction of bulk NiO species. Tada *et al.*[13] reported that the two reduction peaks can be observed at 340 and 420 °C, which were attributed to the reduction of NiO on CeO_2 at about 400 °C. Ding *et al.*[40] also reported that the main reduction peaks appeared at 350–450 °C; these peaks were attributed to the reduction of NiO. In this study, the Ni/CeO_2 catalyst exhibited four-hydrogen-consumption maximum peaks at 165 °C, 225 °C, 290 °C and 785 °C, which were attributed to highly dispersive NiO species or $Ni(OH)_2$, NiO species on the subsurfaces, Ni–O–Ce species, and bulk CeO_2 reduction peaks, respectively. It should be noted that all the reduction peaks are shifted to a lower temperature compared to previously reported studies. It can be suggested that, although the catalytic composition was the same, the reduction trend can differ, depending on the preparation conditions *e.g.*, the kinds of precursor, calcination temperature/time, and metal loadings. For the Ni/Al_2O_3 catalyst, two reduction peaks were observed at 250–400 °C and 400–500 °C. The first peak is assigned to the free Ni species and second peak is attributed to the Ni species combined with the Al_2O_3 support (Ni–O–Al).[40] Evidence from the literature showed that the last reduction peak can be observed for the Ni/Al_2O_3 catalyst in the high-temperature

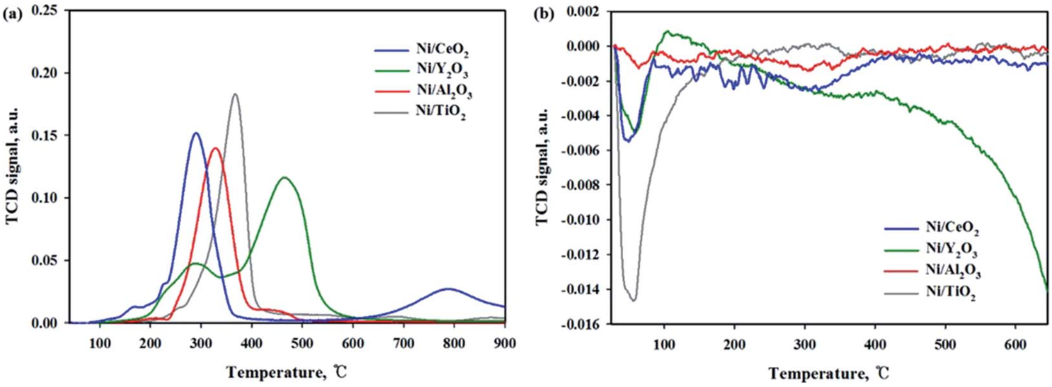

Fig. 5 (a) H_2-TPR and (b) CO_2 TPO profiles of Ni/metal oxide catalysts.

region (750–850 °C), suggesting a stronger interaction between NiO and the Al_2O_3 support.[21] But this peak was not observed in this sample; this might be due to a low calcination temperature. For the Ni/Y_2O_3 catalyst, the two broad reduction peaks were observed in the 200–350 °C and 370–600 °C ranges, respectively. The first peak indicate the existence of a interaction between NiO and the Y_2O_3 support and the second reduction peak is attributed to the bulk Y_2O_3 support. The Ni/TiO_2 catalyst exhibited only one broad hydrogen consumption peak at 250–420 °C, which was attributed to the Ni species combined with the TiO_2 support (Ni–O–Ti). It is expected that the 10 wt% Ni based catalysts may have a metallic Ni form at 420 °C of reduction temperature. According to the H_2 TPR and activity test results of all catalysts, enhancement of the CO_2 conversion could be mainly due to the higher amount of NiO species able to be reduced at low temperature. CO_2 temperature-programmed oxidation (TPO) was performed to observe the CO_2 conversion for reduced catalysts at 420 °C as shown in Fig. 5(b). For the reduced Ni/TiO_2 catalyst, the one huge CO_2 consumption peak was observed in the 50–150 °C. This result indicated that the reduced Ni/TiO_2 catalyst was able to accept oxygen by introduction of CO_2 on reducible sites. However, on the Ni surface H, adsorption is difficult due to low Ni dispersion, which makes it difficult to react the CO_2 methanation. The reduced Ni/CeO_2 and Ni/Y_2O_3 catalysts exhibited the similar CO_2 consumption peak at 50–100 °C. For the reduced Ni/Al_2O_3 catalyst, the CO_2 consumption peak was not observed at all temperature range, it may be concluded that the CO_2 molecules cannot be dissociated on reduced Ni/Al_2O_3 catalyst. Among the catalysts used in this study, the Ni/CeO_2 and Ni/Y_2O_3 catalyst had the higher dispersion and enhanced reducibility of Ni particles, as well as strong metal and support interactions, which could become an important factor for the catalytic activity during low-temperature CO_2 methanation.

3.3 *In situ* DRIFTS

To investigate the interaction of CO_2 with catalysts, *in situ* DRIFT studies were performed on the reduced and unreduced catalysts at 200 and 300 °C as shown in Fig. 6. Fig. 6(a) shows the CO_2 adsorption profile on the Ni/CeO_2 catalyst surface. The assignment of CO_2 adsorption bands for the $Ni/Ce_{0.5}Zr_{0.5}O_2$ catalyst was performed by reported in the previous literature.[41,42] The spectra of CO_2 adsorption on Ni/CeO_2 are similar to those of the $Ni/Ce_{0.5}Zr_{0.5}O_2$ catalyst. The band observed at 1595 cm^{-1} can be assigned to formate species and the bands centered at 1367 cm^{-1} was assigned to monodentate carbonate. These two main bands were still maintained at 300 °C, implying that the formation of formate and monodentate carbonate species are favored at high temperature, as the main intermediate during direct hydrogenation of CO_2.[41,43–46] The reduced and unreduced Ni/CeO_2 catalysts exhibited similar CO_2 adsorption bands, regardless of calcination or reduction treatments, indicating that the CO_2 adsorption properties on Ni/CeO_2 catalyst may depend on the CeO_2 support, not NiO and metallic Ni species. CO_2 adsorption bands were compared for Ni/Y_2O_3 and Ni/Al_2O_3 in Fig. 6(b) and (c). The main adsorption bands were detected at 1541, 1290, 1215 and 1046 cm^{-1} (formate), and 1571 cm^{-1} (bidentate carbonate) for Ni/Y_2O_3 catalyst and at 1606, 1406 and 1364 cm^{-1} (formate), and 1364 cm^{-1} (bidentate carbonate) for Ni/Al_2O_3. The formate bands were maintained at 300 °C for Ni/Al_2O_3 and Ni/Y_2O_3 catalysts. The intensity of main peaks increased with higher temperature (300 °C) for Ni/Al_2O_3 catalyst. In Fig. 6(d), the CO_2 adsorption bands were observed for the Ni/TiO_2 catalyst. The bands centered at 1219 and 1067 cm^{-1} were attributed to monodentate species and the bands centered at 1620 and 1219 cm^{-1} were assigned to hydrogen carbonate peaks. The intensity of CO_2 absorbed peaks decreased at calcined catalyst while these peaks increased with H_2 reduction treatment, indicating that a small part of catalytic sites become active by surface OH groups, and CO_2 adsorption peaks are increased. Fig. 7 shows the CO_2 adsorption profiles of all reduced and unreduced catalysts in the CO_2–$4H_2$ atmosphere as a function of different temperatures. The two main bands attributed to formate and monodentate carbonate were still maintained at 200 and 300 °C for the calcined Ni/CeO_2 catalyst when introducing CO_2 and H_2 (Fig. 7(a)). These peaks were maintained at the reaction temperature of 200 °C for reduced Ni/CeO_2 catalyst but the intensity of peaks decreased obviously at reaction temperature of 300 °C and the two bands were detected at 1900 and 2038 cm^{-1} which was assigned bridged CO and linear CO

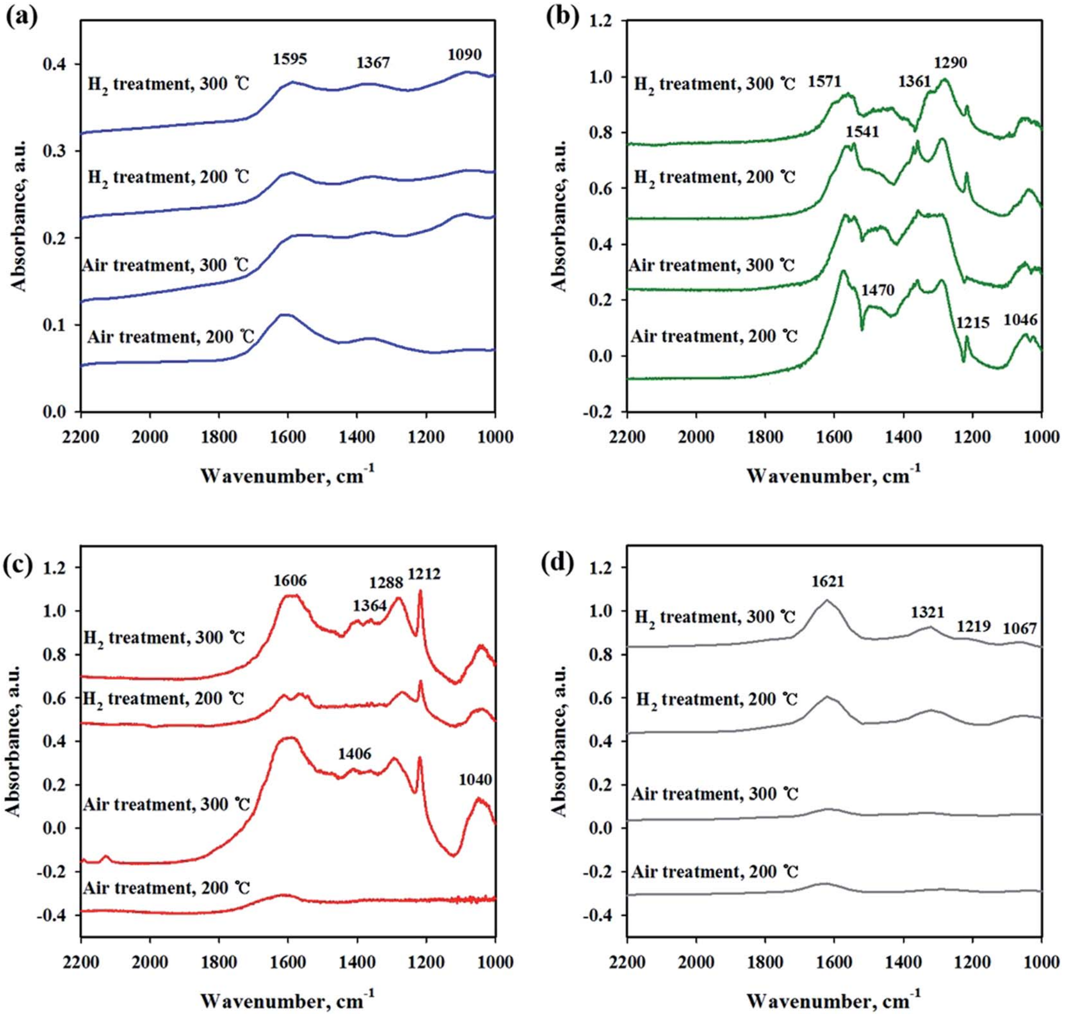

Fig. 6 *In situ* DRIFTS studies of CO_2 adsorption on Ni/metal oxide catalysts with different pretreatment and temperature conditions. (a) Ni/CeO_2, (b) Ni/Y_2O_3, (c) Ni/Al_2O_3 and (d) Ni/TiO_2.

bands adsorbed on Ni, respectively.[47] This result indicated that CO_2 was readily dissociated to CO and it does participate in the CO_2 methanation reaction at high temperature for Ni/CeO_2 catalyst. Aldana *et al.*[44] reported that methanation proceeds through formate species originated from the hydrogenation of carbonates and CO was formed by a redox cycle on reduced ceria support. At 300 °C, only monodentate carbonate bands well remained. This result indicated that the monodentate carbonates are not easily hydrogenated; this result was in good agreement with Pan *et al.*[41] As shown in Fig. 7(b), although hydrogen is injected, the main formate and bidentate carbonate bands were still maintained at 200 and 300 °C for the calcined Ni/Y_2O_3 catalyst. The small and broad formate bands observed at 300 °C for the reduced Ni/Y_2O_3 catalyst and the two small bands were detected at 1900 and 2038 cm^{-1} which was assigned bridged CO and linear CO bands adsorbed on Ni, respectively, it form a similar pattern with reduced Ni/CeO_2 catalyst. This formation of active species as formate leads to higher catalytic activity at high temperature. It is expected that sufficient reduction pretreatment of reducible supports such as CeO_2 and Y_2O_3 supported catalysts efforts on CO_2 decomposition into CO which is an crucial step in CO_2 conversion into CH_4 at high temperature and thus catalytic activity using Ni/CeO_2 and Ni/Y_2O_3 catalysts is enhanced.[13] In Fig. 7(c), the CO_2 absorption bands were still maintained at 200 °C for the calcined Ni/Al_2O_3 catalyst, it forms a similar pattern with CO_2 adsorption pattern as shown in Fig. 6(c). CO_2 methanation is not progressed in this low temperature for Ni/Al_2O_3 catalyst. The similar bands were detected at 300 °C for the calcined Ni/Al_2O_3 catalyst, but the small band observed at 2027 cm^{-1} which was assigned linear CO bands adsorbed on Ni. It is known from the H_2 TPR results that the release of bonding oxygen atoms within Ni–O–Al by H_2 reduction at 300 °C, CO_2 was readily dissociated to CO on reduction active site for the calcined Ni/Al_2O_3 catalyst. The spectra for the reduced Ni/Al_2O_3 catalyst exhibited small overlapped bands of formate species and the intensity of bridged CO and linear CO peaks centered at 1870 and 2027 cm^{-1} increased. This result indicated that CO_2 was readily dissociated to CO and it does participate in the CO_2 methanation reaction at high temperature for reduced Ni/Al_2O_3 catalyst. The Ni/TiO_2 catalyst

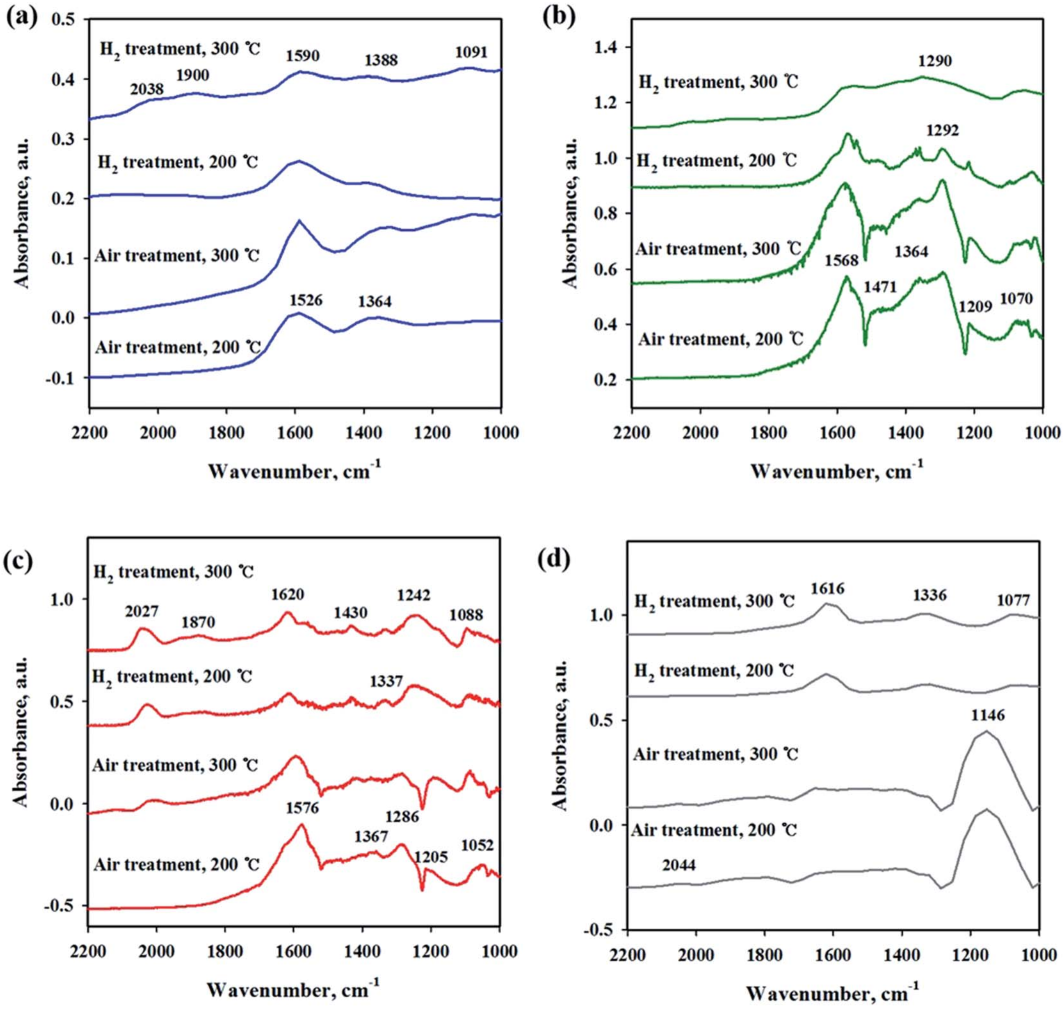

Fig. 7 *In situ* DRIFTS studies of CO_2 methanation ($CO_2 + H_2$) on Ni/metal oxide catalysts with different pretreatment and temperature conditions. (a) Ni/CeO_2, (b) Ni/Y_2O_3, (c) Ni/Al_2O_3 and (d) Ni/TiO_2.

showed a different adsorption bands than other catalyst as shown in Fig. 7(d). The intensity of broad hydrogen carbonate peak centered at 1000–1300 cm^{-1} increased for calcination Ni/TiO_2 catalyst and the two small bands were observed at 1336 and 1077 cm^{-1} which was assigned monodentate peaks regardless of reaction temperature. The amount of CO_2 adsorbed onto Ni/TiO_2 was much larger than that onto other catalyst, but CO_2 methanation reaction cannot occur regardless of reaction temperature. Due to the low Ni dispersion, it can be inferred that adsorbed monodentate and hydrogen carbonate species are difficult to react with adsorbed hydrogen atoms on active metallic Ni site to form methane so that CO_2 methanation reaction does not take place at all temperatures. Numerous studies about reaction mechanism of CO_2 methanation have been investigated. The reaction mechanisms are normally classified into two reaction pathways. One involves CO_2 conversion to CO as intermediate, which then follows the same mechanism as CO methanation.[48] The other one involves formate and carbonate as main intermediate, which directly hydrogenate without forming CO.[44] From the results in this study, it was assumed that the methanation reaction of CO_2 will follow the first mechanism for Ni/Al_2O_3 catalyst and formate and carbonate as main intermediate mechanism at low temperature (200 °C) for Ni/Y_2O_3 and Ni/CeO_2 catalysts. However, the methanation reaction of CO_2 will follow the first mechanism at high temperature (300 °C) for Ni/Y_2O_3 and Ni/CeO_2 catalysts. These different mechanisms might be one of the reasons why the role of supports. The Ni supported irreducible Al_2O_3 catalyst favors the CO_2 conversion to CO and then follows the same mechanism as CO methanation. While carbonate and formate species were found to be the main intermediate on surface oxygen vacancy site such as Ce^{3+} sites, which could enhance the catalytic activity at low temperature compare to Ni/Al_2O_3 catalyst.[3] The carbonate and formate species were mainly present as an adsorption intermediate on surface oxygen vacancy site (Ce^{3+} sites), while the CO species were found to be the main adsorption intermediate for the irreducible Al_2O_3 supported Ni catalyst. According to TPR and DRIFT results, the interaction between Ni and Ce or Y may facilitate the formation of the OH groups on the Ni–OH or Y–OH, Ce–OH bonds. The dissociated hydrogen atoms on the Ni metal spillover onto the ceria or yttria support surface, and undergo surface diffusion at low temperature by introduction of hydrogen. Superior reducibility of both Ni-rich surface species and CeO_2 support by strong interaction between Ni and CeO_2 or Y_2O_3 supports are important factor and then weakly adsorbed CO_2 species such as formate and carbonate on the surface oxygen vacancy site easily reacted with hydrogen dissociation on the metal followed by spillover at low temperature.

4 Conclusions

The Ni/CeO_2 and Ni/Y_2O_3 catalysts show highly enhanced catalytic activity for low-temperature CO_2 methanation, as compared with the Ni/Al_2O_3 and Ni/TiO_2 catalysts. The increase in the low-temperature CO_2 methanation activity can be directly correlated with an enhancement in the reducibility and small Ni particle size of the Ni/CeO_2 and Ni/Y_2O_3 catalyst, which is caused by a strong interaction between reduced CeO_2 or Y_2O_3 oxide support and Ni. When Ni species are dispersed on "reducible" oxides, such as CeO_2 and Y_2O_3, carbonate and formate species were mainly present as an adsorption intermediate on the surface oxygen vacancy site such as $Y^{(3-x)+}$ or Ce^{3+} sites at low temperature, which plays a key role in enhancing the low catalytic activity. Due to the low Ni dispersion of Ni/TiO_2 catalyst, it can be concluded that adsorbed CO_2 species are difficult to react with hydrogen atoms on active metallic Ni site to form methane. When the Ni species were dispersed on "irreducible" oxides, species such as Al_2O_3 and CO were found to be the main adsorption intermediates. Overall, CeO_2 and Y_2O_3 supports are promising support for the Ni-based catalyst and further improvement in low-temperature CO_2 methanation activity can be made by modification of the mixed CeO_2 and Y_2O_3 support with small Ni particle size and oxygen vacancies.

Author contributions

Ye Hwan Lee: conceptualization, writing – original draft. Jeong Yoon Ahn: experiment and evaluation. Dinh Duc Nguyen: data curation, validation, formal analysis. Soon Woong Chang: writing – review & editing. Sung Su Kim: writing – review & editing. Sang Moon Lee: supervision, project administration.

Conflicts of interest

There are no conflicts to declare.

Acknowledgements

This research was supported by Basic Science Research Program through the National Research Foundation of Korea (NRF) funded by the Ministry of Education (2017R1D1A1B03036192).

Notes and references

1 F. Ocampo, B. Louis, L. Kiwi-Minsker and A. C. Roger, *Appl. Catal., A*, 2011, **392**, 36–44.
2 K. Ghaib, K. Nitz and F.-Z. Ben-Fares, *ChemBioEng Rev.*, 2016, **3**, 266–275.
3 M. A. A. Aziz, A. A. Jalil, S. Triwahyono and A. Ahmad, *Green Chem.*, 2015, **17**, 2647–2663.
4 Q. Pan, J. Peng, T. Sun, D. Gao and S. Wang, *Fuel Process. Technol.*, 2014, **123**, 166–171.
5 W. J. Shen, M. Okumura, Y. Matsumura and M. Haruta, *Appl. Catal., A*, 2001, **213**, 225–232.
6 V. M. Shinde and G. Madras, *AIChE J.*, 2014, **60**, 1027–1035.
7 M. Yamasaki, H. Habazaki, T. Yoshida, E. Akiyama, A. Kawashima, K. Asami, K. Hashimoto, M. Komori and K. Shimamura, *Appl. Catal., A*, 1997, **163**, 187–197.
8 G. D. Weatherbee and C. H. Bartholomew, *J. Catal.*, 1981, **68**, 67–76.
9 M. Yamasaki, H. Habazaki, K. Asami, K. Izumiya and K. Hashimoto, *Catal. Commun.*, 2006, **7**, 24–28.
10 A. E. Aksoylu and Z. I. Önsan, *Appl. Catal., A*, 1997, **164**, 1–11.
11 F. Ocampo, B. Louis and A. C. Roger, *Appl. Catal., A*, 2009, **369**, 90–96.
12 X. Zhang, W. J. Sun and W. Chu, *J. Fuel Chem. Technol.*, 2013, **41**, 96–101.
13 S. Tada, T. Shimizu, H. Kameyama, T. Haneda and R. Kikuchi, *Int. J. Hydrogen Energy*, 2012, **37**, 5527–5531.
14 N. Takezawa, H. Terunuma, M. Shimokawabe and H. Kobayashib, *Appl. Catal.*, 1986, **23**, 291–298.
15 K. Zhao, W. Wang and Z. Li, *J. CO_2 Util.*, 2016, **16**, 236–244.
16 H. Muroyama, Y. Tsuda, T. Asakoshi, H. Masitah, T. Okanishi, T. Matsui and K. Eguchi, *J. Catal.*, 2016, **343**, 178–184.
17 G. Zhou, H. Liu, K. Cui, A. Jia, G. Hu, Z. Jiao, Y. Liu and X. Zhang, *Appl. Surf. Sci.*, 2016, **383**, 248–252.
18 J. Liu, C. Li, F. Wang, S. He, H. Chen, Y. Zhao, M. Wei, D. G. Evans and X. Duan, *Catal. Sci. Technol.*, 2013, **3**, 2627–2633.
19 E. Jwa, S. B. Lee, H. W. Lee and Y. S. Mok, *Fuel Process. Technol.*, 2013, **108**, 89–93.
20 J. Ashok, M. L. Ang and S. Kawi, *Catal. Today*, 2017, **281**, 304–311.
21 S. Abate, C. Mebrahtu, E. Giglio, F. Deorsola, S. Bensaid, S. Perathoner, R. Pirone and G. Centi, *Ind. Eng. Chem. Res.*, 2016, **55**, 4451–4460.
22 S. Damyanova, B. Pawelec, R. Palcheva, Y. Karakirova, M. C. C. Sanchez, G. Tyuliev, E. Gaigneaux and J. L. G. Fierro, *Appl. Catal., B*, 2018, **225**, 340–353.
23 P. Frontera, A. Macario, M. Ferraro and P. L. Antonucci, *Catalysts*, 2017, **7**, 1–28.
24 T. A. Le, M. S. Kim, S. H. Lee, T. W. Kim and E. D. Park, *Catal. Today*, 2017, **293–294**, 89–96.
25 S. Abelló, C. Berrueco and D. Montané, *Fuel*, 2013, **113**, 598–609.
26 C. Vogt, E. Groeneveld, G. Kamsma, M. Nachtegaal, L. Lu, C. J. Kiely, P. H. Berben, F. Meirer and B. M. Weckhuysen,

Unravelling structure sensitivity in CO_2 hydrogenation over nickel, *Nat. Cat.*, 2018, **1**, 127–134.

27 Y. Yan, Y. Dai, H. He, Y. Yu and Y. Yang, *Appl. Catal., B*, 2016, **196**, 108–116.

28 D. Wierzbicki, R. Baran, R. Dębek, M. Motak, M. E. Gálvez, T. Grzybek, P. Da Costa and P. Glatzel, *Appl. Catal., B*, 2018, **232**, 409–419.

29 K. Ray and G. Deo, *Appl. Catal., B*, 2017, **218**, 525–537.

30 W. Cai, Q. Zhong and Y. Zhao, *Catal. Commun.*, 2013, **39**, 30–34.

31 M. Guo and G. Lu, *Catal. Commun.*, 2014, **54**, 55–60.

32 A. Trovarelli, *Catalysis by ceria and related materials*, World Scientific Publishing Co., Singapore, 2002.

33 F. T. Zangeneh, S. Sahebdelfar and M. T. Ravanchi, *J. Nat. Gas Chem.*, 2011, **20**, 219–231.

34 H. Zhang, Y. Dong, W. Fang and Y. Lian, *Chin. J. Catal.*, 2013, **34**, 330–335.

35 H. Singh, A. Rai, R. Yadav and A. K. Sinha, *Mol. Catal.*, 2018, **451**, 186–191.

36 S. Hwang, J. Lee, U. G. Hong, J. H. Baik, D. J. Koh, H. Lim and I. K. Song, *J. Ind. Eng. Chem.*, 2013, **19**, 698–703.

37 J. Ren, X. Qin, J. Z. Yang, Z. F. Qin, H. L. Guo, J. Y. Lin and Z. Li, *Fuel Process. Technol.*, 2015, **137**, 204–211.

38 B. Mutz, H. W. P. Carvalho, S. Mangold, W. Kleist and J. D. Grunwaldt, *J. Catal.*, 2015, **327**, 48–53.

39 Y. Zeng, H. Ma, H. Zhang, W. Ying and D. Fang, *Fuel*, 2015, **162**, 16–22.

40 M. Ding, J. Tu, Q. Zhang, M. Wang, N. Tsubaki, T. Wang and L. Ma, *Biomass Bioenergy*, 2016, **85**, 12–17.

41 Q. Pan, J. Peng, S. Wang and S. Wang, *Catal. Sci. Technol.*, 2014, **4**, 502–509.

42 S. Tada, O. J. Ochieng, R. Kikuchi, T. Haneda and H. Kameyama, *Int. J. Hydrogen Energy*, 2014, **39**, 10090–10100.

43 S. Sharma, Z. Hu, P. Zhang, E. W. Mcfarland and H. Metiu, *J. Catal.*, 2011, **278**, 297–309.

44 P. A. U. Aldana, F. Ocampo, K. Kobl, B. Louis, F. Thibault-Starzyk, M. Daturi, P. Bazin, S. Thomas and A. C. Roger, *Catal. Today*, 2013, **215**, 201–207.

45 Q. Pan, J. Peng, T. Sun, S. Wang and S. Wang, *Catal. Commun.*, 2014, **45**, 74–78.

46 C. Schild, A. Wokaun and A. Baiker, *J. Mol. Catal.*, 1990, **63**, 223–242.

47 S. ichiro Fujita, M. Nakamura, T. Doi and N. Takezawa, *Appl. Catal., A*, 1993, **104**, 87–100.

48 A. Beuls, C. Swalus, M. Jacquemin, G. Heyen, A. Karelovic and P. Ruiz, *Appl. Catal., B*, 2012, **113–114**, 2–10.